Comparison of OVERFLOW Computational and Experimental Results for a Blunt Mars Entry Vehicle Concept During Supersonic Retropropulsion

Logan D. Halstrom*, Thomas H. Pulliam† , Robert E. Childs‡ , and Paul M. Stremel§, and Patrick J. Moran¶
NASA Ames Reseach Center, Moffett Field, CA, 94035

Simulations of supersonic retropropulsion (SRP) flow over a Hypersonic Inflatable Aerodynamic Decelerator (HIAD) blunt-body vehicle were performed using the OVERFLOW Computational Fluid Dynamics (CFD) solver. Simulation conditions and geometry were designed to match specific test runs in the Descent System Study (DSS) testing campaign. The relative accuracy of simulation predictions are assessed by direct comparison to experimental data. Computational predictions of the SRP flowfield and bow shock shape are compared to experimental schlieren images. Comparisons of the model surface pressure environment are presented for unsteady and static discrete tap data as well as time-averaged Pressure-sensitive Paint (PSP) data.

Nomenclature

Symbols

C_D	=	drag force coefficient
C_P	=	pressure coefficient
C_T	=	thrust coefficient
C_v	=	thermal energy coefficient
L/D	=	lift-to-drag ratio
M	=	Mach number
Re	=	Reynolds number
α	=	angle of attack
$w.r.t.$	=	with respect to

Acronyms

AETC	=	Aerosciences Evaluation and Test Capabilities
AMR	=	Adaptive Mesh Refinement
BC	=	boundary condition
CC	=	compressibility correction
CFD	=	Computational Fluid Dynamics
DES	=	Detached Eddy Simulation
DSS	=	Descent System Study

*Aerospace Engineer, Systems Analysis Office (ARC-AA), AIAA Member, logan.halstrom@nasa.gov
†Senior Research Scientist, Science & Technology Corporation, AIAA Associate Fellow
‡Senior Research Scientist, Science & Technology Corporation
§Senior Research Scientist, Science & Technology Corporation, AIAA Member
¶Computer Scientist, Advanced Computing Branch (ARC-TNC)

EDL	=	Entry, Descent, and Landing
	=	
HIAD	=	Hypersonic Inflatable Aerodynamic Decelerator
HLLC	=	Harten-Lax-van Leer-Contact
HLLE++	=	Harten-Lax-van Leer-Einfeldt
LUPWT	=	Langley Unitary Plan Wind Tunnel
NASA	=	National Aeronautics and Space Administration
PSP	=	Pressure-sensitive Paint
QCR	=	Quadratic Constitutive Relation
RANS	=	Reynolds-averaged Navier-Stokes
RC	=	rotation and curvature
SRP	=	supersonic retropropulsion
SSOR	=	Symmetric Successive Over-Relaxation
SST	=	Shear Stress Transport
STMD	=	Space Technology Mission Directorate

I. Introduction

HUMAN exploration of Mars is an ongoing focus of science and technology development at the National Aeronautics and Space Administration (NASA) and other organizations. One of the key remaining technical challenges in active development is the ability to safely and reliably land significantly large payloads on the planet's surface. The Martian atmosphere has a relatively low average density, which diminishes the effectiveness of aerodynamic drag deceleration techniques traditionally employed for Earth atmospheric reentry, but still requires shielding from aerothermodynamic heating and active control during powered descent. Recent NASA robotics missions have successfully employed a combination of a hypersonic aeroshell, a supersonic parachute, and a subsonic retropropulsion and sky-crane manuever for Martian Entry, Descent, and Landing (EDL). However, NASA's critical mission requirement for future EDL vehicles is a payload capacity on the order of twenty metric tons, which is twenty times greater than current capabilities. These future missions, which include both precursor robotic and follow-on human landings, will forego the use of parachutes for supersonic deceleration due to the prohibitively large canopy sizes that would be required for these heavy-mass payloads. Instead, these missions will rely on powered descent or supersonic retropropulsion (SRP) for the latter stages of Martian EDL [1, 2]. One such vehicle concept is the low-L/D Hypersonic Inflatable Aerodynamic Decelerator (HIAD) [3], depicted in Fig. 1. This concept features a deployable aeroshell that enables traditional aerodynamic deceleration from orbital velocity to $M \sim 2$, after which SRP engines integrated into the structure are used for final deceleration and landing.

Development of these concept vehicles requires a fundamental understanding of the complex aerodynamics associated with SRP, which can be challenging to obtain. A typical SRP flowfield is characterized by a bow shock supported by back-pressure from turbulent jets, which often results in unsteady fluctuations of the shock shape. Between the bow shock and vehicle surface is a complex environment of rocket plume shear layers interacting with mixed regions of strong normal shocks and weak oblique shocks that can dramatically alter the dynamic pressure in the post-shock region. Ground testing of these complex flows requires innovative model design and sophisticated data acquisition techniques. Additionally, the actual conditions of hot jets in the low-pressure, low-density, primarily-CO_2 Martian atmosphere are difficult to recreate in ground testing on Earth. Computational Fluid Dynamics (CFD) is a powerful tool that offers unique abilities to enhance and expand upon the SRP testing capabilities of traditional wind tunnel facilities. However, accurate simulation of the full complexity of SRP flow requires exceptional rigor in the application of CFD modeling best practices for spatial resolution and temporal convergence, and experimental validation is key for calibrating and establishing quantifiable computational accuracy.

An extensive campaign of SRP wind tunnel testing and analogous CFD simulation has been conducted under the NASA Aerosciences Evaluation and Test Capabilities (AETC) portfolio office to assess the relative merits of supersonic wind tunnel testing and CFD methods for fulfilling future aerodynamic data-generation needs. A primary criterion is the ability of CFD to provide vehicle aerodynamics data that is of "sufficient accuracy and reliability" to that produced by wind tunnel experiments. Ross et al. give a description of the objectives and scope of this effort [5]. One component

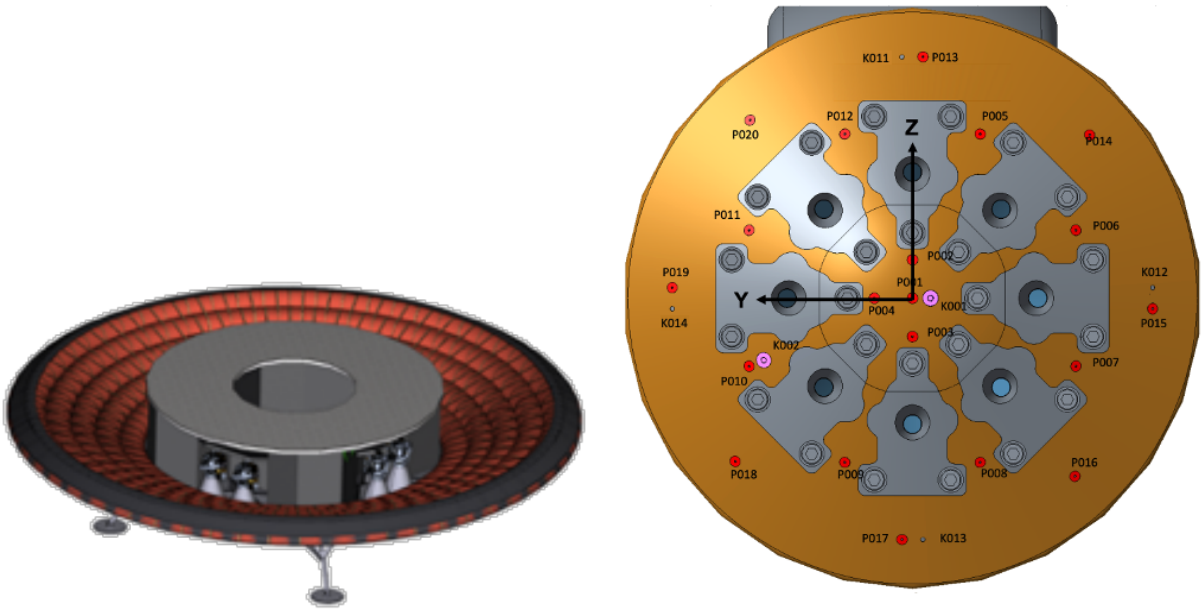

(a) Artist concept [1] **(b) Wind tunnel test model [4]**

Fig. 1 Concept Low-L/D HIAD Mars EDL vehicle for human exploration missions

of this testing campaign is the study of SRP on the HIAD concept vehicle in partnership with the Descent System Study (DSS) under the Game Changing Development (GCD) program of NASA's Space Technology Mission Directorate (STMD). This paper describes predictions of the aerodynamics of the HIAD concept using the OVERFLOW CFD solver and provides comparisons of these results to experimental data. It is published as part of a special AIAA session, which includes an overview of the experiment [6] that was conducted in the spring of 2023 and of the results simulated with OVERFLOW and several other CFD solvers [7] in conjunction with the wind tunnel test. The special session also contains an additional specific analysis using OVERFLOW for the mid-L/D CobraMRV concept vehicle [8] and a summary for best practices in simulating SRP flows with OVERFLOW [9].

Section II of this paper summarizes the CFD solver parameters and computational domain utilized for the simulations presented in this work. Section III discusses the SRP flow behaviors observed in the OVERFLOW HIAD simulations and provides comparisons between computational and experimental results for unsteady aerodynamics (high-frequency schlieren imaging and Kulite® pressure tap data), steady aerodynamics (static pressure tap and Pressure-sensitive Paint (PSP) data), and balance-measured and integrated loads on the vehicle model.

II. Computational Methodology

A. Numerical Methods

CFD simulations were performed using OVERFLOW, which is an implicit Navier-Stokes solver that employs finite-differencing methods on structured, overset grids [10–13]. Overset grid systems were developed using Chimera Grid Tools (CGT) [14–16] and its associated Graphic User Interface (GUI) Overgrid [15]. Overset region communication, interpolation stencils, and cell blanking were computed using Domain Connectivity Function (DCF) [17, 18].

All solutions were computed using a time-accurate solver with five Newton sub-iterations at each time step to improve convergence. Time step size was determined by successively decreasing the step size until the general unsteady flow behavior remained consistent between changes, which corresponded to a non-dimensional value of 0.5 for these simulations. Inner-iteration convergence was assessed for each solution to ensure accurate numerics. Time was advanced implicitly using Symmetric Successive Over-Relaxation (SSOR), and the Harten-Lax-van Leer-Contact (HLLC) upwind spatial discretization scheme was employed throughout the tunnel test section and near-body region. Alternatively, the Harten-Lax-van Leer-Einfeldt (HLLE++) upwind scheme was applied locally in the bow shock region to provide more

accurate shock capturing.

All simulations were initially converged with the two-equation Shear Stress Transport (SST) Reynolds-averaged Navier-Stokes (RANS) turbulence model [19], as it has been shown to be more accurate than other models available in OVERFLOW for flows with rocket plumes and other significant non-wall-bounded shear layers, such as the Orion Launch Abort Vehicle and re-entry crew module, for which extensive experimental data was available for model validation [20, 21]. Time-accurate RANS or Unsteady Reynolds-averaged Navier-Stokes (URANS) is more computationally efficient than higher-order turbulence modeling methods, such as Detached Eddy Simulation (DES), often by an order of magnitude, and it was of interest to assess the relative accuracy of URANS in modeling SRP flow compared to other methods.

Additionally, specific turbulence modeling options were found to be critical for obtaining the best possible CFD accuracy for SRP applications. It was found that the combination of enabling the rotation and curvature (RC) option and disabling the compressibility correction (CC) option produced the most realistic predictions for SRP flow [9]. For the underexpanded rocket plumes typical of this application, the RC option is prone to under-predicting shear layer growth in these barrel-shaped shear layers. In practice, this deficiency was compensated for by disabling the CC option (even though high-Mach number flows usually benefit from the CC option). Though this combination is not suitable for all types of high speed jets, it works well for the underexpanded ones modeled in this work. It was also found that the Quadratic Constitutive Relation (QCR) model [22, 23] is beneficial in corner regions of the wind tunnel but has adverse effects in plumes. Again leveraging OVERFLOW's ability to permit the use of different model options on different grids, QCR was enabled in the grids that carry the bulk of the wall flow, including its corners, but QCR is disabled in all grids near the vehicle. Additional detail on DSS SRP solution sensitivity to the OVERFLOW solver parameters discussed above can be found in the OVERFLOW simulation guidelines paper by Matsuno et al..

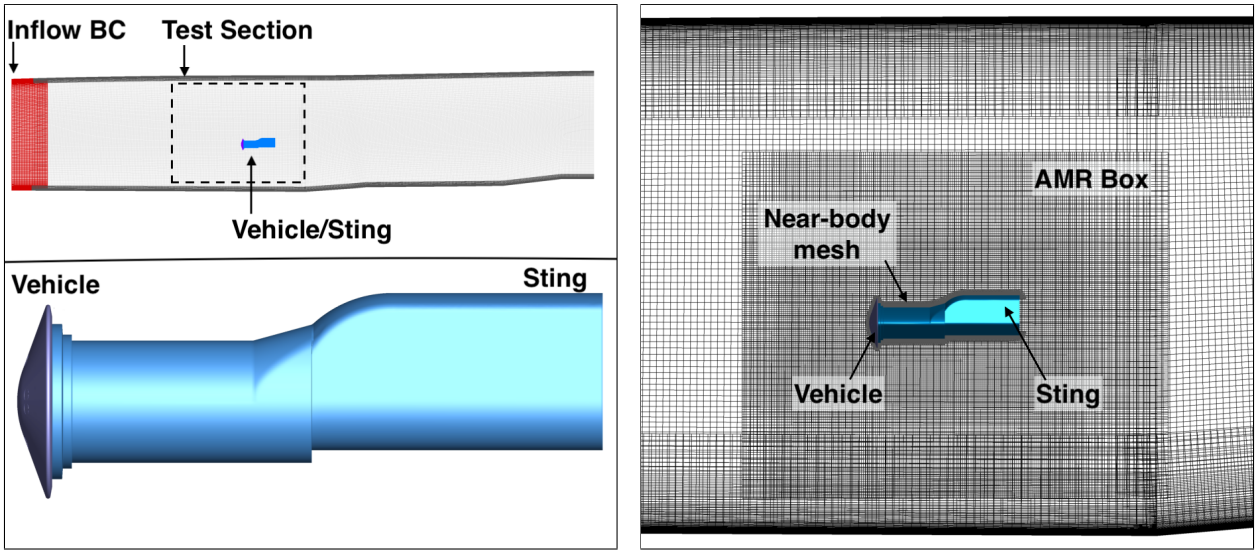

(a) Wind tunnel test section boundary conditions and vehicle surface geometry

(b) Near-body volume grid and overlaid shock/plume refinement box

Fig. 2 HIAD/LUPWT overset grid system for OVERFLOW SRP simulations

B. Overset Grid System

The overset grid system for the CFD simulations conducted for this work consists of a segment of the Langley Unitary Plan Wind Tunnel (LUPWT) geometry containing the test section and the HIAD vehicle mounted to a truncated representation of the wind tunnel sting, as depicted in Fig. 2. The inflow boundary condition (BC) to the test section grid is derived from a simulation of the "full-empty-tunnel", as described below, and is prescribed at the constant-x plane indicated in Fig. 2a, which is twenty heatshield diameters forward of the vehicle model. Exit flow is modeled over an additional twenty-two diameters through the aft geometry of the wind tunnel test section, which contains two pressure-recovery compression ramps. The vehicle and sting near-body volume grids are encompassed in a surrounding coarse box grid, within which Adaptive Mesh Refinement (AMR) is activated to refine the mesh locally in regions

where SRP flow features like the rocket plumes and bow shock are computed.

In initial simulations with the LUPWT geometry, it was found that the test section flow cannot be idealized by neglecting the inflow boundary layers and subtle nonuniformity of the true test section flow. The upwash angle of the flow due to the upstream asymmetric wind tunnel nozzle-block expansion was shown to be as great as one degree in magnitude, and there are also weak, wake-like features from hardware in the settling chamber that survive passage through the wind tunnel nozzle-block throat and influence the test section flow. Thus, the inflow BC to the test section for use in the DSS vehicle CFD work was obtained from simulations of the "full" wind tunnel geometry with an empty test section, which were performed by several groups in the AETC effort, including calculations done with OVERFLOW [24]. In the full-empty-tunnel simulations, the truncated LUPWT circuit was extended to include the settling chamber upstream of the test section, with internal geometry features of approximately one inch or larger modeled. Multiple instantaneous solutions at the inflow plane to the test section were extracted and averaged to produce a steady CFD approximation of the true flow into the test section, which was used as the inflow BC for the test section-only simulations conduced for this paper.

III. Results and Comparisons

This section reports the post-test OVERFLOW CFD results for the HIAD 1E and 1F nozzle configurations. It identifies the specific SRP flow phenomena for this application and provides qualitative and quantitative comparisons between simulation and experiment.

A. Unsteady Supersonic Retropropulsion Flowfield

Notable flow unsteadiness was observed at many test conditions and was characterized by dynamic bow shock shape modulations that resulted in both high-frequency fluctuations and long-period modulations of the surface pressure distribution.

1. Schlieren Comparisons

This section will provide qualitative comparisons of computational and experimental unsteady and averaged schlieren results. Bow shock shape and SRP shock-plume interaction structures predicted by time-accurate CFD shows qualitative similarity to experimental results, as can be seen in the instantaneous flow comparisons in Fig. 3. Experimental results at the pre-test CFD condition of $\alpha = 10^\circ$ exhibited poor visibility of the SRP flow structure, so the mirror condition of $\alpha = -10^\circ$ is shown, and post-test simulations will be performed to match this condition for a more direct comparison. Current comparisons show a similar bow shock standoff distance and similar asymmetry in the bow shock shape punctuated by a shock triple point due to non-zero angle of attack (α).

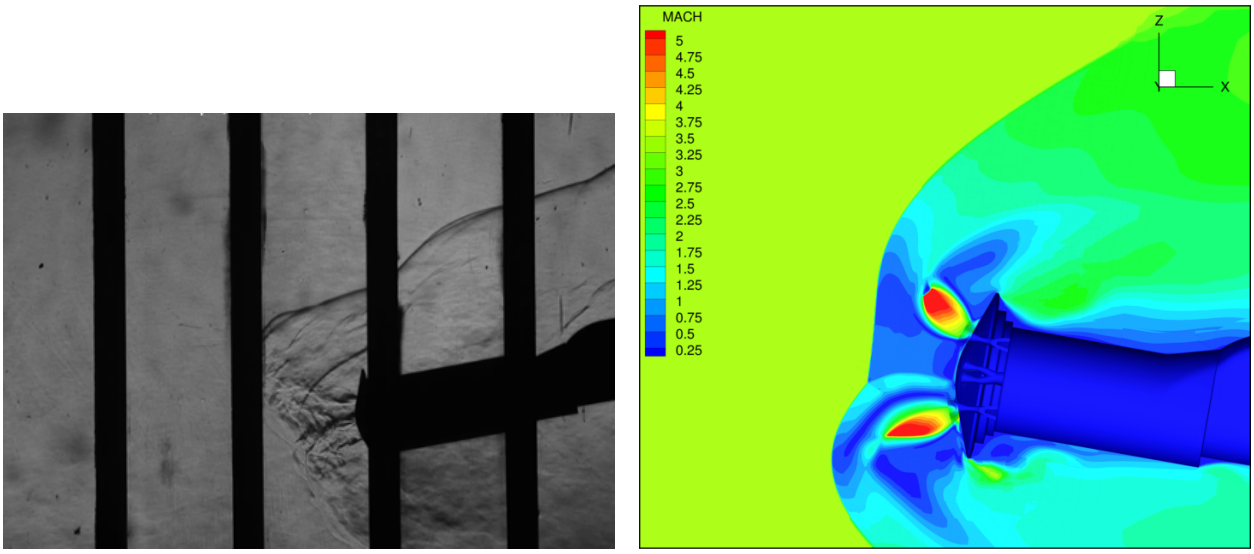

(a) Instantaneous experimental schlieren imaging ($M = 3.49, C_T = 0.93, \alpha = -10°$)

(b) Pre-test RANS CFD centerline Mach number contours ($M = 3.5, C_T = 1.0, \alpha = 10°$)

Fig. 3 Comparison of the experimental and computational instantaneous SRP flowfield

2. Unsteady Pressure Tap Comparisons

This section compares simulation surface pressure coefficient (C_P) unsteadiness to experimental data measured by high-frequency Kulite® pressure sensors. Signal unsteadiness was more significant at non-zero α. Pressure signal standard deviation is presented in Fig. 4, where direct comparisons between simulation and experiment show that CFD predictions using FUN3D (F3D) DES turbulence modeling are more accurate in predicting flow unsteadiness magnitude compared to OVERFLOW (OVF) RANS results. Based on results for the CobraMRV [9], similar improvements in accuracy are expected for the post-test OVERFLOW DES simulations of the HIAD that will be included as part of the final paper.

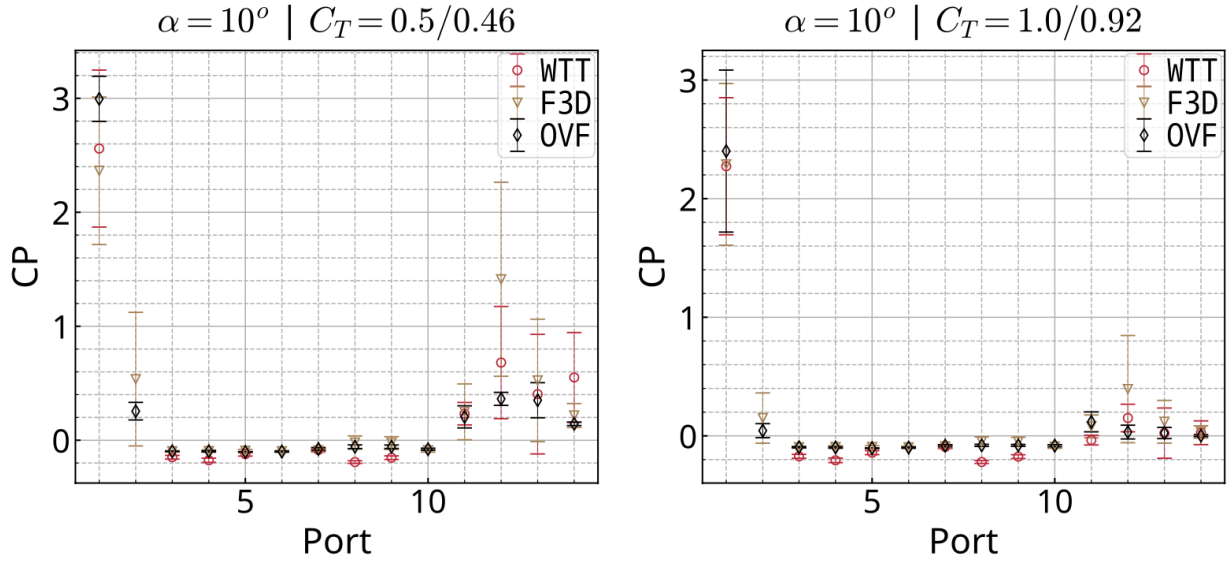

Fig. 4 Comparison of pretest CFD to discrete measurements of unsteady surface pressure

B. Mean Supersonic Retropropulsion Flowfield

1. Static Pressure Tap Comparisons

This section compares discrete measurements of averaged surface C_P. As with the schlieren results in Section III.A.1, CFD results utilizing FUN3D (F3D) DES turbulence modeling are seen to be more similar in magnitude to the experiment than pre-test OVERFLOW (OVF) RANS simulations. Post-test OVERFLOW DES simulations, to be included in the final paper, are expected to show similarly improved comparison to experiment. The final paper will also identify trends with respect to (*w.r.t.*) α and thrust coefficient (C_T), and will also compare differences between the HIAD 1E and 1F nozzle configurations.

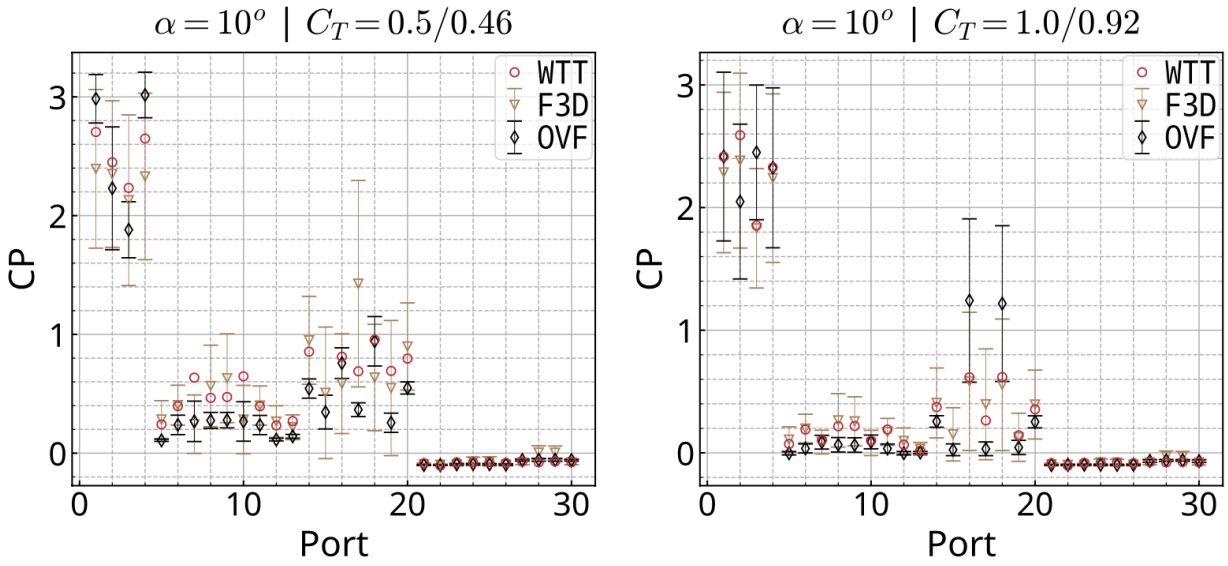

Fig. 5 Comparison of pretest CFD and experimental mean static pressure tap data

2. Pressure-sensitive Paint Comparisons

This section will compare PSP measurements of averaged surface C_P distribution to computational predictions. It should be noted that there is significant calibration error associated with the experimental results due to variations in the surface material on and around removable inserts, which affects both the local calibration in specific areas (such as inboard of the nozzles) as well as the global calibration magnitude. The final paper will address the accuracy of the quantitative comparisons between experiment and simulation.

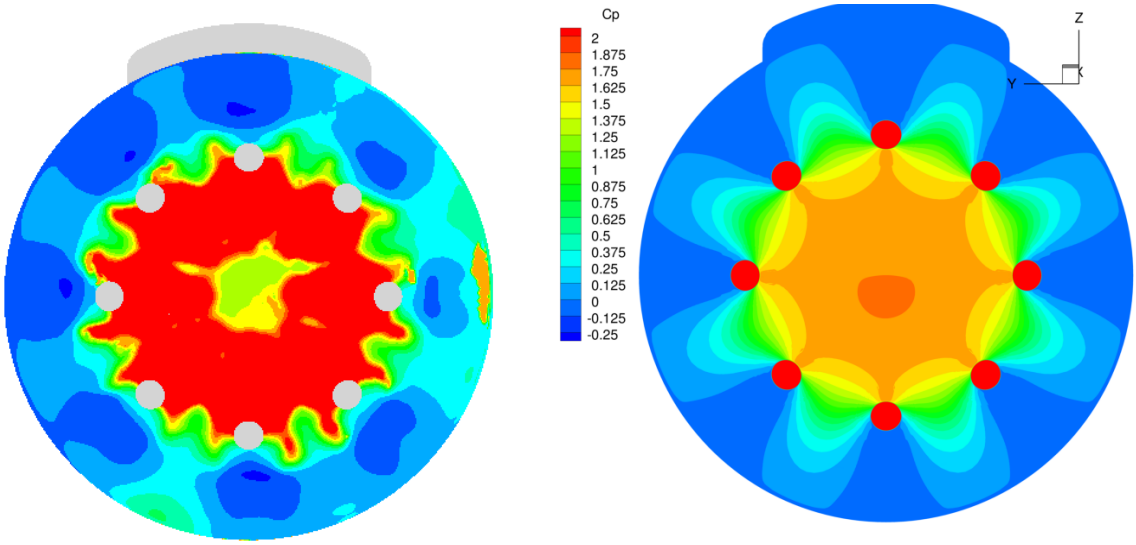

(a) Averaged experimental Pressure-sensitive Paint imaging ($M = 3.49, C_T = 2.0, \alpha = -10°$)

(b) Pre-test RANS CFD heatshield surface C_P contours ($M = 3.5, C_T = 2.5, \alpha = 10°$)

Fig. 6 Comparison pretest CFD and preliminary experimental heatshield surface pressure distributions

IV. Conclusion

This paper will provide comparisons of simulated SRP conditions of the HIAD Mars EDL concept vehicle to experimental results. The qualitative similarity of the SRP flowfield will be assessed by direct comparison of computational and experimental schlieren imaging. The quantitative accuracy of CFD predictions of SRP flow unsteadiness will be assessed by statistical comparison with high-frequency pressure tap data. Comparisons of averaged simulation surface C_P to experimental static tap data will demonstrate surface pressure prediction accuracy, and will be further corroborated with PSP comparisons. CFD integrated aerodynamic loads will also be compared to balance-measured loads. Finally, the trade study between the accuracy and computational efficiency of RANS vs. DES turbulence modeling applied to SRP flow will be assessed through experimental comparison.

Acknowledgments

This work is supported by the joint effort between NASA's Aerosciences Evaluation and Test Capabilities (AETC) program office under the Aeronautics Research Mission Directorate (ARMD) and the Game Changing Development (GCD) program's Descent System Study (DSS) under the Space Technology Mission Directorate (STMD). CFD simulations were run on NASA Advanced Supercomputing Division resources and were funded by the GCD program's DSS. The authors thank the AETC and DSS teams for their advice and collaboration and J. Garcia and K. Matsuno for their review of this research.

References

[1] Cianciolo, A., Korzun, A., Samareh, J., Sostaric, R., Calderon, D., and Garcia, J., "Human Mars Entry, Descent, and Landing Architecture Study: Phase 3 Summary," 2020.

[2] Cerimele, C. J., Robertson, E. A., Sostaric, S. R., Campbell, C. H., Robinson, P., Matz, D. A., Stachowiak, S. J., Garcia, J. A., Bowles, J. V., Kinney, D. J., and Theisinger, J. E., "A rigid mid-lift-to-drag ratio approach to human Mars entry, descent, and landing," *AIAA Guidance, Navigation, and Control Conference*, 2017, p. 1898.

[3] Cianciolo, A. D., Dillman, R., Brune, A., Lugo, R., Polsgrove, T., Percy, T. K., Sutherlin, S., and Cassell, A., "Human Mars Entry, Descent and Landing Architecture Study: Deployable Decelerators," *AIAA SPACE*, 2018.

[4] Edquist, K. T., "Status of Mars Retropropulsion Testing in the Langley Unitary Plan Wind Tunnel," *Submitted to AIAA Scitech 2022 Forum*, 2022.

[5] Ross, J. C., Rhode, M. N., Falman, B., Edquist, K., Schoenenberger, M., Brauckmann, G. J., Kleb, W. L., West, T., Alter, S. J., and Witte, D., "Evaluation of CFD as a Surrogate for Wind-Tunnel Testing for Mach 2.4 to 4.6-Project Overview," *AIAA AVIATION 2021 FORUM*, 2021, p. 2961.

[6] Edquist, K. T., Falman, B. E., Burns, D. E., Watkins, A. N., Pham, H. T., and Houlden, H. P., "Testing of Two Mars Powered Descent Vehicle Concepts in the Langley Unitary Plan Wind Tunnel," *AIAA Aviation Forum*, 2024.

[7] Edquist, K., Glass, C., Korzun, A., Wood, W., West, T., Alter, S., Canabal, F., Childs, R., Halstrom, L., and Matsuno, K., "Computational Analysis of Two Mars Powered Descent Vehicle Concepts Tested in the Langley Unitary Plan Wind Tunnel," *AIAA Aviation Forum*, 2024.

[8] Matsuno, K., Childs, R., Pulliam, T., Stremel, P., Garcia, J., and Moran, P., "Comparison of OVERFLOW Computational and Experimental Results of the CobraMRV Mars Entry Vehicle Concept during Supersonic Retropropulsion," *Submitted to AIAA Aviation 2024 Forum*, 2024.

[9] Matsuno, K., Halstrom, L., Pulliam, T., Childs, R., Stremel, P., Garcia, J., and Moran, P., "OVERFLOW Guidelines for Simulation of Supersonic Retropropulsion," *Submitted to AIAA Aviation 2024 Forum*, 2024.

[10] Buning, P. G., "NASA OVERFLOW CFD Code," `https://overflow.larc.nasa.gov/`, 2021. Accessed: 2021-05-20.

[11] Buning, P. G., Jespersen, D. C., Pulliam, T. H., Chan, W., Slotnick, J. P., Krist, S., and Renze, K. J., "Overflow user's manual," *NASA Langley Research Center, Hampton, VA*, 2002.

[12] Nichols, R., Tramel, R., and Buning, P., "Solver and turbulence model upgrades to OVERFLOW 2 for unsteady and high-speed applications," *24th AIAA Applied Aerodynamics Conference*, 2006, p. 2824.

[13] Nichols, R. H., and Buning, P. G., "User's Manual for OVERFLOW 2.1," *University of Alabama and NASA Langley Research Center*, 2008.

[14] Rogers, S., Roth, K., Nash, S., Baker, M., Slotnick, J., Whitlock, M., and Cao, H., "Advances in overset CFD processes applied to subsonic high-lift aircraft," *18th Applied Aerodynamics Conference*, 2000, p. 4216.

[15] Chan, W., "The overgrid interface for computational simulations on overset grids," *32nd AIAA Fluid Dynamics Conference and Exhibit*, 2002, p. 3188.

[16] Chan, W., "Developments in Strategies and Software Tools for Overset Structured Grid Generation and Connectivity," *20th AIAA Computational Fluid Dynamics Conference*, 2011, p. 3051.

[17] Meakin, R., "Object X-rays for cutting holes in composite overset structured grids," *15th AIAA Computational Fluid Dynamics Conference*, 2001, p. 2537.

[18] Chan, W. M., Kim, N., and Pandya, S. A., "Advances in domain connectivity for overset grids using the x-rays approach," 2012.

[19] Menter, F. R., "Two-equation eddy-viscosity turbulence models for engineering applications," *AIAA journal*, Vol. 32, No. 8, 1994, pp. 1598–1605.

[20] Childs, R., Garcia, J., Melton, J., Rogers, S., Shestopolov, A., and Vicker, D., "Overflow Simulation Guidelines for Orion Launch Abort Vehicle Aerodynamic Analyses," *29th AIAA Applied Aerodynamics Conference*, 2011, p. 3163.

[21] Childs, R. E., Garcia, J. A., Rogers, S. E., and Vicker, D. J., "Overflow Aerodynamic Simulation of the Orion Launch Abort Vehicle," *Joint Army Navy NASA Air Force*, 2013.

[22] Mani, M., Babcock, D., Winkler, C., and Spalart, P., "Predictions of a supersonic turbulent flow in a square duct," *51st AIAA Aerospace Sciences Meeting including the New Horizons Forum and Aerospace Exposition*, 2013, p. 860.

[23] Spalart, P. R., "Strategies for turbulence modelling and simulations," *International journal of heat and fluid flow*, Vol. 21, No. 3, 2000, pp. 252–263.

[24] Childs, R., Stremel, P., Hawke, V., Garcia, J., Kleb, W. L., Hunter, C., , Parikh, P., Patel, M., Alter, S. J., Rhode, M. N., and Salari, K., "Flow Characterization of the NASA Langley Unitary Plan Wind Tunnel, Test Section 2: Computational Results," *AIAA AVIATION 2021 FORUM*, 2021, p. 2963.